Biological Membranes

DOI: 10.1002/anie.201106482

Electrodeposition of Single-Metal Nanoparticles on Stable Protein 1 Membranes: Application of Plasmonic Sensing by Single Nanoparticles**

*Li-Xia Qin, Yang Li, Da-Wei Li, Chao Jing, Bao-Qin Chen, Wei Ma, Arnon Heyman, Oded Shoseyov, Itamar Willner, He Tian, and Yi-Tao Long**

Organizing biomaterials, such as proteins, on surfaces is one of the challenging goals of bio-nanotechnology.[1] Biological membranes supported on substrates are widely used to mimic the dynamics and structural features of cell membranes,[2,3] and proteins embedded in them could carry out a wide range of physiological and biochemical processes. For example, biosensors can be designed by the incorporation of ion-channel proteins as well as other membrane protein receptors.[4–6] The use of hybrid bilayer membranes (HBMs) that spontaneously coat a covalently tethered hydrophobic layer on metals with a monolayer of solvent-free lipids, has opened up a new era in biomimetic model membranes.[7,8] Although HBM strategies are diverse and well-established,[9] there are only few examples that show the embedding of ion-channel proteins into a HBM system on self-assembled interfaces for in situ monitoring the behavior of single nanoparticles (NPs).[10]

Plasmonics is an emerging sub-field of nanophontonics, which has attracted increasing attention because of its potential applications in controlling and manipulating light at nanoscale dimensions.[11] The advences in dark field microscopy (DFM) enabled the use of this technique to probe plasmonic effects at single NP level, and particularly to examine sizes, shapes, and chemical environments of the NPs. Specifically, the method was implemented to probe biorecognition events and the dynamics of biomolecules.[12–14] Plasmonic metal NPs have great potential for chemical and biological sensor applications, because of their sensitive response to the local environment and the ease of monitoring the strong light or absorbance by the NPs.[15–19] These unique properties suggest the possibility of tuning desired plasmon resonance scattering properties of NPs at the single NP level, and probing the sizes and shapes of single NPs.[20] Although chemical synthesis of colloidal NPs with a range of particle sizes have been reported,[21,22] it is still a challenge to monitor in situ and real time the growth of single NPs by single-particle spectroscopy on a self-assembled template.

The crystal structure of ring-like stable protein 1 (SP1) reveals a ring diameter of 11 nm, an inner pore of 2–3 nm, and a width of 4–5 nm (Scheme 1a).[23–25] SP1 was recently proposed as a new self-assembled molecular scaffold or

[*] L.-X. Qin, Dr. Y. Li, Dr. D.-W. Li, C. Jing, B.-Q. Chen, W. Ma, Prof. H. Tian, Prof. Y.-T. Long
Key Laboratory for Advanced Materials &
Department of Chemistry
East China University of Science and Technology
Shanghai, 200237 (P.R. China)
E-mail: ytlong@ecust.edu.cn
Dr. A. Heyman, Prof. O. Shoseyov
The Robert H. Smith Institute of Plant Sciences
and Genetics in Agriculture
Faculty of Agricultural, Food and Environmental Quality Sciences
The Hebrew University of Jerusalem
Rehovot, 76100 (Israel)
Prof. I. Willner
Institute of Chemistry, The Center for Nanoscience
and Nanotechnology, The Hebrew University of Jerusalem
Jerusalem, 91904 (Israel)

[**] This research was supported by the National Science Found for Distinguished Young Scholars (grant number 21125522), the National Natural Science Foundation of China (grant numbers 91027035 and 21105028), the Fundamental Research Funds for the Central Universities (grant number WK1013002), and the SRFDP (grant number 20100074120017).

Supporting information for this article including preparation methods of small unilamellar vesicles, modification procedures, electrochemical methods, characterization methods, single nanoparticle DFM imaging, and scattering spectroscopy is available on the WWW under http://dx.doi.org/10.1002/anie.201106482.

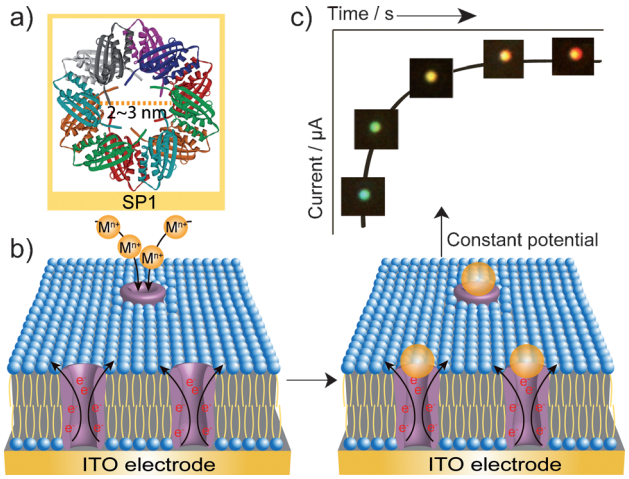

Scheme 1. Electrodeposition in the SP1 generated nanochannels, and Ag, Au, and Cu NPs deposited on the SP1-HBM/ITO template using a developing solution of $AgClO_4$, $HAuCl_4$, and $CuSO_4$ with the standard deposition potentials of −0.05 V, −0.05 V, and −0.6 V vs. Ag/AgCl, respectively. a) Structure of SP1. b) SP1-HBM/ITO template. c) The images of typical color changes of a single Ag NP changing from blue to red, as the electrodeposition time is increased, indicating the in situ and real time monitoring of the growth process of single NPs on the SP1-HBM/ITO template.

nanoscale templates for nano-biotechnological applications. The wild type SP1 (wtSP1) assembles into protein chain structures forming nanotubes and nanoarrays.[26] SP1 and its derivatives have been used to generate hydrophilic nanochannels in the plasma membrane of living cells, and they were covalently linked to various surfaces, that facilitate the assembly of neuroelectronic hybrid systems.[27]

Herein, we implement single NP scattering spectroscopy and electrochemistry for in situ monitoring the growth of Ag, Au, and Cu single NPs on a self-assembled SP1 template on indium–tin oxide (ITO) surfaces (Scheme 1b). We use DFM with a true color imaging charge-coupled device (CCD) camera and a spectrometer (see Figure S1 in the Supporting Information) to follow these processes. We show the images of progressive growth of single Ag, Au, and Cu NPs on the SP1-HBM/ITO template by following the red-shift of the plasmon resonance Rayleigh scattering (PRRS) spectra (λ_{max}) corresponding to the color changes of the different sized metal NPs (Scheme 1c).

Figure S2a in the Supporting Information shows the AFM image of SP1. This image shows that the height of SP1 is about 4.9 nm (in the inset). This value is in good agreement with the value of 4–5 nm reported from the crystal structure. Control experiments of the AFM images (see Figure S2b in the Supporting Information) indicate that SP1 self-assembles with phospholipid layers. The TEM images show the uniform distribution of SP1 (see Figure S2c in the Supporting Information) and bare phospholipid layers (see Figure S2d in the Supporting Information) without SP1, also indicate that SP1 is self-assembled with phospholipid layers. The properties of SP1-HBM/ITO and HBM/ITO template were further characterized by electrochemical Faradaic impedance spectroscopy (EIS)[28,29] and cyclic voltammetry (CV, see Figure S3a in the Supporting Information). At bare ITO, only a very small semicircle is observed, indicating a very small electron transfer resistance R_{et} of about 12 Ω (curve 1). Silanization of the ITO surface with triethoxy (octy) silane/acetone solution generated an insulating layer on the electrode surface, which increased the electron transfer resistance (R_{et}) value of 31 Ω (curve 2). The semicircle diameter of the Nyquist plot increased significantly and the R_{et} value increased to 540 Ω upon functionalization of the silanized ITO with HBM (curve 3). After doping of the membrane with SP1, the semicircle diameter of the Nyquist plot decreased, and the R_{et} value was reduced to 135 Ω (curve 4), indicating that the membrane turned porous toward the transport of the redox label. By fitting the EIS spectra with an electronic circuit, the values of C_m for HBM/ITO and for SP1-HBM/ITO corresponded to 10.7 and 20.5 μF cm^{-2}, respectively, indicating that doping the HBM with the porous SP1 channels resulted in a net decrease of electron transfer resistance. The corresponding CVs of bare ITO (1), silanized ITO (2), HBM/ITO (3), and SP1-HBM/ITO (4) in a 1 mM ferricyanide solution are illustrated in Figure S3b in the Supporting Information. While the deposition of HBM on the ITO prohibited the electrical contact between the redox label $Fe(CN)_6^{3-/4-}$, the deposition of SP1 on the membrane yields pores that facilitate electron transfer between the redox label and the electrode support.

The Ag, Au, and Cu nanoclusters were electrodeposited in the SP1 pores by the reduction of $AgClO_4$ (10^{-5} M), $HAuCl_4$ (10^{-5} M), and $CuSO_4$ (10^{-3} M) at a standard deposition potentials of −0.05 V, −0.05 V, and −0.6 V versus Ag/AgCl on the SP1 (3×10^{-6} M)-HBM/ITO support. Figure 1 shows the reflectance spectra of single Ag (a), Au (b), and Cu (c) NPs. As the time interval of electrodeposition time is prolonged (from 0 to 30 min), the λ_{max} values are shifted to longer wavelengths from 528 to 647 nm, from 560 to 620 nm, and from 530 to 570 nm for Ag, Au, and Cu NPs, respectively. The corresponding typical color changes of single Ag, Au, and Cu NP are displayed in the insets. Moreover, SEM images characterized the growth process of single NPs (see Figure S4 in the Supporting Information), upon increasing the electrodeposition time for 5 and 25 min, the surface coverage of the enlarged Ag, Au, and Cu single NPs on the SP1-HBM/ITO interface also increases, with the particles exhibiting dimen-

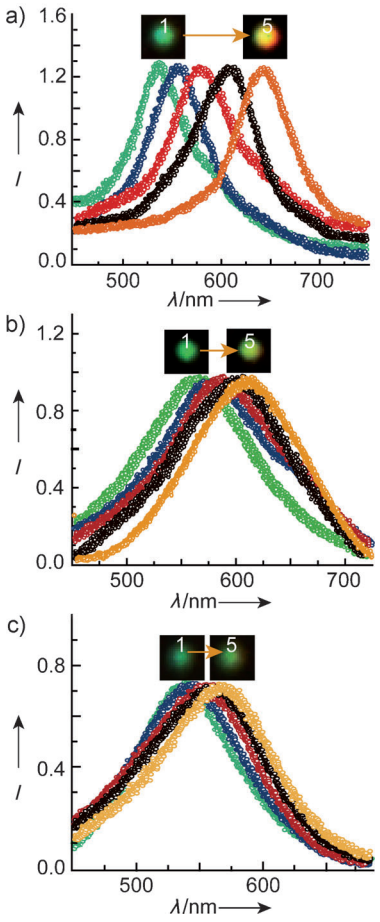

Figure 1. Typical time-dependent scattering spectra of a) single Ag, b) Au, and c) Cu (1–5) shifted to longer wavelengths observed upon the electrodeposition of the NPs from $AgClO_4$, $HAuCl_4$, and $CuSO_4$ solutions on the SP1-HBM/ITO template for time intervals of electrodeposition corresponding to a) 5, b) 10, c) 15, d) 20, and e) 25 min. (The intensities *I* of all scattering spectra have been normalized). The inset shows the typical color images of a single Ag NP changing from green to red, a single Au NP changing from green to yellow, and a single Cu NP changing from green to cyan where the initial images were recorded after 5 min (1) and the final images were recorded after 25 min (5).

sions of 46.6 nm (a1) and 75.8 nm (a5), 52.3 nm (b1) and 71.5 nm (b5), and 39.9 nm (c1) and 49.4 nm (c5), respectively. Actually, Cu(0) is prone to surface oxidation upon the exposure to ambient atmosphere at room temperature, the PRRS spectra of the Cu nanosphere and the optical properties of the Cu NP arrays are significantly affected by the presence of copper oxides.[30] It was found that removal of the Cu oxides with glacial acetic acid yielded a dramatic difference in the observed PRRS spectra, as shown in Figure S5 in the Supporting Information. Several control experiments confirm that the electrodeposition of the Ag, Au, and Cu nanoclusters proceed selectively on the SP1 pores. We find that no electrodeposition of metallic NPs occurred on the HBM/ITO support, that lacked SP1 (see respective SEM images on Figure S6, a1, b1, and c1 and DFM images in Figure S6, a2, b2, and c2 in the Supporting Information). Also, on the bare ITO electrode we find that thick and inhomogeneous metal aggregates were formed after 1 min of electrodeposition, and they could be imaged by DFM (see Figure S6, a3, b3, and c3 in the Supporting Information). Furthermore, the interparticle spacing was modulated by controlling the loading of SP1 on the HBM (see Figure S7 in the Supporting Information).

For further support the Ag, Au, and Cu NPs were electrodeposited in the pores, SP1 was labeled with a fluorephore and the modified support was imaged simultaneously by fluorescence microscopy and DFM. The SP1 was modified with the fluorescent dye Cy3 and the labelled protein was incorporated into the HBM. The embedded protein was imaged by fluorescence microscopy (see Figure 2a). After electrodeposition of the Ag, Au, and Cu NPs, the fluorescence/DFM images revealed bright NPs in the center of the fluorescent protein, implying that the NPs are, indeed, deposited in the pore cores of the protein (Figure 2b, c, and d).

The PRRS shifts of the metallic NPs are sensitive to dielectric changes or refractive index changes, occurring at the interface of the NPs. Accordingly, the association of molecules or biomolecules on the NPs can be assayed by following the PRRS shifts.[31,32] In fact, the time-dependent PRRS shifts, as a result of the association of a host substrate, may also be implemented to follow the dynamics of binding of the molecule/biomolecule to the NPs. Thus, PRRS may be used to develop sensors that probe recognization events at the single NP level. This concept was used to follow by PRRS antibody–antigen interactions at the single NP level. HED10 is an autoimmune antibody (IgG) that specificity binds poly(dT).[33–35] Accordingly, the thiolated poly(dT) was assembled on the different metals deposited on the SP1 pores. The fragment (Fab) of the HED10 antibody was then linked to the $poly(dT)_{50}$ antigen associated with the Ag, Au, and Cu/SP1-HBM/ITO surfaces. Figure 3 shows the PRRS spectra shifted to longer wavelengths by $\Delta\lambda_{max}$ for HS-$poly(dT)_{50}$ observed upon the attachment of Ag (a), Au (b), and Cu (c) NPs. The $\Delta\lambda_{max}$ corresponding to 7.9 nm (from 1 to 2), 5.8 nm (from 1 to 2), and 4.5 nm (from 1 to 2), respectively. Subsequently, the Fab HED10 (10^{-5} M) antibody was injected into the HS-$poly(dT)_{50}$ antigen-functionalized NPs solution. As shown in Figure 3, the PRRS spectra are further shifted to longer wavelengths corresponing to $\Delta\lambda = 23.7$ nm for the Ag NP (from 2 to 3), $\Delta\lambda = 17.1$ nm for the Au NP (from 2 to 3), and $\Delta\lambda = 10.3$ nm for the Cu NPs (from 2 to 3). Control experiments revealed that no significant PRRS spectral shifts were observed upon interaction of HED10 with HS-poly(dA) or HS-poly(dC)-functionalized Ag, Au, and Cu NPs (Figure S8a, b, c, and d, e, f in the Supporting Information). These results showed that the PRRS spectral shifts in the presence of the HS-$poly(dT)_{50}$ antigen and HED10 antibody originate from specific antigen–antibody interactions. The PRRS spectral shifts, $\Delta\lambda_{max}$, upon binding of the Fab HED antibody to the $poly(dT)_{50}$ antigen can also be used for the quantitative assay of antigen–antibody interactions at the single NP label. Figure 3d shows the spectral shifts of individual Ag, Au, and Cu NPs modified with the $poly(dT)_{50}$ antigen at variable concentrations of the Fab HED10. The $\Delta\lambda_{max}$ value increased as the concentration of the antibody was elevated within the concentration range of 10^{-8}–10^{-5} M. At higher concentrations, the $\Delta\lambda_{max}$ value reached saturation, consistent with the saturation of the antigen site by the antibody. Furthermore, the spectral shifts $\Delta\lambda_{max}$ upon binding the antibody are highest for the Ag NPs and lowest for the Cu NPs, consistent with the plasmonic properties of the different NPs shown in Figure 1. Thus, the results showed that PRRS can be implemented to quantitatively analyse antigen–antibody recognition events at the single NP level. The significance of these results rests on the fact that the method can be applied to analyze very small sample volumes.

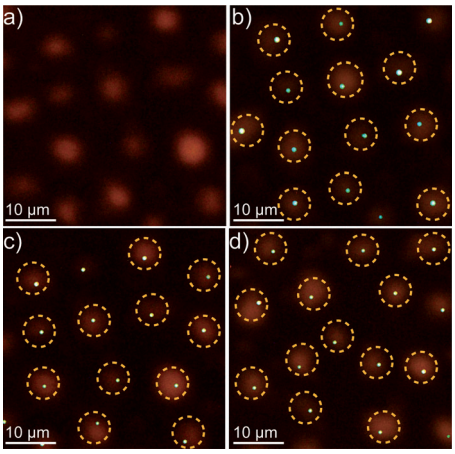

Figure 2. Fluorescence microscopy images of the Cy3-labeled SP1 on the HBM/ITO support: HBM/ITO (a) and the corresponding DFM images of deposited Ag (b), Au (c), and Cu (d) NPs on the SP1-HBM/ITO template.

In conclusion, in the present study electrochemical methods and dark field microscopy are used to follow the in situ formation of Ag, Au, and Cu NPs on SP1 pore proteins integrated in a HBM membrane associated on an ITO electrode. The PRRS spectral shifts make it possible to monitor the time-dependent growth of NPs at the single NP level. The study confirmed that the electrodeposition of the NPs occurs only on the SP1 pore. Also, the PRRS spectral shifts make it possible to probe recognition binding events at the single NP level, thus paving the way to develop a new sensing and biosensing platform.

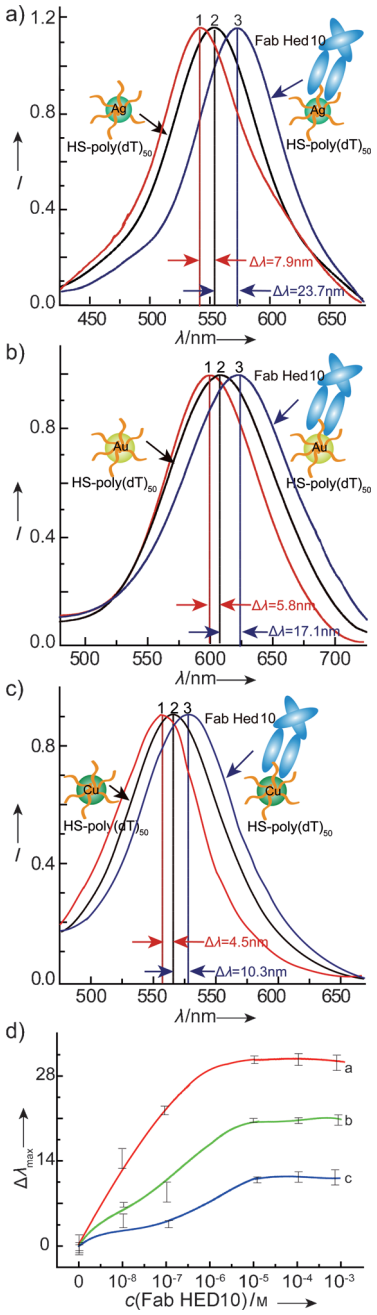

Figure 3. Spectral shifts of single NPs with similar size and shape upon binding of HS-poly(dT)$_{50}$ and Fab HED10. The PRRS spectra corresponding to a) single Ag, b) Au, and c) Cu particles (1 in red), PRRS spectra after adsorption of 10 μM HS-poly(dT)$_{50}$ onto a) the Ag, b) Au, and c) Cu NPs (2 in black), and PRRS spectra after functionalization of the HS-poly(dT)$_{50}$ NPs with Fab HED10 (3 in blue). d) Scattering spectra of poly(dT)$_{50}$ attached to the Ag, Au, and Cu NPs as a function of the Fab HED10 concentrations of 10^{-8}, 10^{-7}, 10^{-5}, 10^{-4}, and 10^{-3} M. The error bars show standard deviations of five replicate tests.

Received: September 13, 2011
Revised: October 31, 2011
Published online: November 21, 2011

Keywords: dark-field microscopy · electrochemistry · membranes · plasmon resonance Rayleigh scattering · proteins

[1] S. Mann, *Nat. Mater.* **2009**, *8*, 781.
[2] S. M. Butterfield, H. A. Lashuel, *Angew. Chem.* **2010**, *122*, 5760; *Angew. Chem. Int. Ed.* **2010**, *49*, 5628.
[3] R. Ranganathan, *Science* **2007**, *318*, 1253.
[4] B. A. Cornell, V. L. B. Braach-Maksvytis, L. G. King, P. D. J. Osman, B. Raguse, L. Wieczorek, R. J. Pace, *Nature* **1997**, *387*, 580.
[5] F. M. Menger, A. L. Galloway, M. E. Chlebowski, S. Wu, *J. Am. Chem. Soc.* **2006**, *128*, 14034.
[6] H. M. Keizer, B. R. Dorvel, M. Andersson, D. Fine, R. B. Price, J. R. Long, A. Dodabalapur, I. Kper, W. Knoll, P. A. V. Anderson, R. S. Duran, *ChemBioChem* **2007**, *8*, 1246.
[7] G. Favero, L. Campanella, S. Cavallo, A. D'Annibale, M. Perrella, E. Mattei, T. Ferri, *J. Am. Chem. Soc.* **2005**, *127*, 8103.
[8] A. Devadoss, J. D. Burgess, *J. Am. Chem. Soc.* **2004**, *126*, 10214.
[9] A. Hosseini, J. P. Collman, A. Devadoss, G. Y. Williams, C. J. Barile, T. A. Eberspacher, *Langmuir* **2010**, *26*, 17674.
[10] C. C. Hayden, J. S. Hwang, E. A. Abate, M. S. Kent, D. Y. Sasaki, *J. Am. Chem. Soc.* **2009**, *131*, 8728.
[11] C. F. Chen, S. D. Tzeng, H. Y. Chen, K. J. Lin, S. Gwo, *J. Am. Chem. Soc.* **2008**, *130*, 824.
[12] Y. Li, C. Jing, L. Zhang, Y.-T. Long, *Chem. Soc. Rev.* **2011**, DOI: 10.1039/c1s15143f.
[13] T. Huang, P. D. Nallathamby, D. Gillet, X.-H. N. Xu, *Anal. Chem.* **2007**, *79*, 7708.
[14] L. Zhang, Y. Li, D.-W. Li, C. Jing, X. Chen, M. Lv, Q. Huang, Y.-T. Long, I. Willner, *Angew. Chem.* **2011**, *123*, 6921; *Angew. Chem. Int. Ed.* **2011**, *50*, 6789.
[15] J. Zhao, L. Jensen, J. Sung, S. L. Zou, G. C. Schatz, R. P. Van Duyne, *J. Am. Chem. Soc.* **2007**, *129*, 7647.
[16] E. Ozbay, *Science* **2006**, *311*, 189.
[17] M. L. Tran, S. P. Centeno, J. A. Hutchison, H. Engelkamp, D. Liang, G. V. Tendeloo, B. F. Sels, J. Hofkens, H. Uji-I, *J. Am. Chem. Soc.* **2008**, *130*, 17240.
[18] S. K. Tapan, C. J. Murphy, *J. Am. Chem. Soc.* **2004**, *126*, 8648.
[19] A. J. Haes, R. P. Van Duyne, *J. Am. Chem. Soc.* **2002**, *124*, 10596.
[20] Y. I. Yang, E. Jeong, I. Choi, S. Lee, H. D. Song, K. Kim, Y. Choi, T. Kang, J. Yi, *Angew. Chem.* **2011**, *123*, 4614; *Angew. Chem. Int. Ed.* **2011**, *50*, 4520.
[21] Y. Khalavka, J. Becker, C. Sönnichsen, *J. Am. Chem. Soc.* **2009**, *131*, 1871.
[22] T. Thurn-Albrecht, J. Schotter, G. A. Kastle, N. Emley, T. Shibauchi, L. Krusin-Elbaum, K. Guarini, C. T. Black, M. T. Tuominen, T. P. Russel, *Science* **2000**, *290*, 2126.
[23] W. X. Wang, O. Dgany, O. Dym, A. Altman, O. Shoseyov, O. Almog, *Acta Crystallogr. Sect. D* **2003**, *59*, 512.
[24] W. X. Wang, D. Pelah, T. Alergand, O. Shoseyov, A. Altman, *Plant Physiol.* **2002**, *130*, 865.
[25] O. Dgany, A. Gonzalez, O. Sofer, W. X. Wang, G. Zolotnitsky, A. Wolf, Y. Shoham, A. Altman, S. G. Wolf, O. Shoseyov, O. Almog, *J. Biol. Chem.* **2004**, *279*, 51516.
[26] I. Medalsy, O. Dgany, M. Sowwan, H. Cohen, A. Yukashevska, S. G. Wolf, A. Wolf, A. Koster, O. Almog, I. Marton, Y. Pouny, A. Altman, O. Shoseyov, D. Porath, *Nano Lett.* **2008**, *8*, 473.
[27] A. Khoutorsky, A. Heyman, O. Shoseyov, M. E. Spira, *Nano Lett.* **2011**, *11*, 2901.
[28] H. T. Yuan, H. Shimotani, J. T. Ye, S. Yoon, H. Aliah, A. Tsukazaki, M. Kawasaki, Y. Iwasa, *J. Am. Chem. Soc.* **2010**, *132*, 18402.
[29] G. P. Kissling, C. Bünzli, D. J. Fermín, *J. Am. Chem. Soc.* **2010**, *132*, 16855.
[30] J. H. Kim, S. H. Ehrman, T. A. Germer, *Appl. Phys. Lett.* **2004**, *84*, 1278.

[31] J. S. Lee, D. F. Dombroski, T. R. Mosmann, *Biochemistry* **1982**, *21*, 4940.
[32] M. Barry, C. Mol, W. Anderson, J. S. Lee, *J. Biol. Chem.* **1994**, *269*, 3623.
[33] S. L. Kleinman, J. M. Bingham, A. I. Henry, K. L. Wustholz, R. P. Van Duyne, *Proc. SPIE* **2010**, *7757*, 77570J.
[34] Y. L. Ying, D. W. Li, Y. Li, J. S. Lee, Y.-T. Long, *Chem. Commun.* **2011**, *47*, 5690.
[35] A. D. McFarland, R. P. Van Duyne, *Nano Lett.* **2003**, *3*, 1057.

